Thin-Walled Structures 104 (2016) 71–81

Contents lists available at ScienceDirect

Thin-Walled Structures

journal homepage: www.elsevier.com/locate/tws

Full length article

Optimal design of composite thin-walled beams using simulated annealing

Florencia Reguera [a,b,c,*], Víctor Hugo Cortínez [a,b,c,*]

[a] Centro de Investigación en Mecánica Teórica y Aplicada, Universidad Tecnológica Nacional, FRBB, 11 de Abril 461, B8000LMI Bahía Blanca, Argentina
[b] Consejo Nacional de Investigaciones Científicas y Técnicas, Argentina
[c] Departamento de Ingeniería, Universidad Nacional del Sur, Argentina

ARTICLE INFO

Article history:
Received 15 December 2015
Received in revised form
27 February 2016
Accepted 3 March 2016
Available online 12 March 2016

Keywords:
Thin-walled
Composite beams
Optimal design

ABSTRACT

In this paper, a problem formulation and solution methodology for optimal design of thin-walled composite beams is presented. The aim is to maximize the buckling load capacity and minimize the weight of the beam. For this purpose, a theoretical model is developed for the analysis of thin-walled composite beams under a state of arbitrary initial stresses. In order to find the optimal solution, Simulated Annealing method is implemented. Design variables are taken as the stacking sequences of laminate and the dimensions of the cross-section. The space of feasible solutions is constrained by strength, displacements, global and local buckling and geometric conditions.

1. Introduction

Composite materials are mostly used in applications where stiffness-to-weight or strength-to-weight ratios are critical. The design of composite structures is a difficult task due to the numerous design variables which have to be simultaneously taken into account. For example varying fiber orientation in each ply, or in a certain number of plies, can produce a large number of acceptable designs that support a specific loading condition. Hence it is necessary to find the structure with the best configuration for a specific application. This can be achieved through a process of optimization design. In the last years many works have been developed related to the optimization of composite structures [1–4]. In addition, another challenge to face is represented by the fact that in engineering practice the design variables are not continuous. Thus, design variables can only take values from a predefined discrete set. Therefore, in order to find the absolute optimum of an objective function a global optimization method must be employed. Stochastic optimization techniques are suitable for this propose, because they can search into a large solution space and escape from local optimum points.

The design of thin-walled composite beams is a very important topic in construction engineering. One-dimensional models are suitable for optimization problems since they capture the main features of the structure behavior, while they are simple enough to be employed in extensive computation. Many one-dimensional models have been developed and implemented [5–9]. A very important aspect in the behavior of composite beams is the shear flexibility due to non-uniform torsional warping. This has been considered in a complete form in several works [10–13]. Additionally, the local buckling must be regarded on the design [14,15]. The local buckling analysis of composite beams is accomplished by modeling the flanges and the webs individually, considering the flexibility of the flange-web connections. Qiao and Shan developed analytical predictions for local buckling of some FRP (Fiber Reinforced Plastic) beams considering the elastic restraints of the flange-web connections [16]. Tarján et al. extended this work to include other boundary conditions and analyzed local buckling analysis of orthotropic composite beams [17].

In the present study, a solution methodology for minimum weight and maximum global buckling load of orthotropic thin-walled beams, with open or closed cross-sections, is developed. The corresponding design variables are given by the dimensions of the cross-section, the thickness of each layer, the fiber orientation of each layer and the number of layers of the laminate. The set of constraints includes global and local stability conditions, strength condition and technological and constructional requirements in the form of geometric relations. A theoretical model for the stability analysis of composite thin-walled beams is proposed to find these conditions. This model incorporates in a full form the shear

* Corresponding authors at: Centro de Investigaciones en Mecánica Teórica y Aplicada, Universidad Tecnológica Nacional, FRBB, 11 de Abril 461, B8000LMI Bahía Blanca, Argentina.
E-mail addresses: freguera@frbb.utn.edu.ar (F. Reguera), vcortine@frbb.utn.edu.ar (V.H. Cortínez).

http://dx.doi.org/10.1016/j.tws.2016.03.001
0263-8231/

flexibility (bending and non-uniform warping effects) and takes into account an arbitrary state of initial stresses. Also, a finite element with two nodes and seven degrees-of-freedom per node is employed to solve the governing equations. Moreover, analytical solutions of the problem of local buckling of orthotropic beams subjected to linearly varying axial loads are employed to impose a local buckling condition. Finally, Simulated Annealing method is applied to find the optimal fiber orientation of the laminates and the cross-section dimensions.

2. Optimal design

In order to find the optimal design which satisfies specific structural conditions a mathematical model of the optimization problem is proposed. The aim is to maximize the global buckling load and minimize the weight of the beam at the same time. To carry out both targets, a dimensionless objective function is assumed to be in the following form [18]

$$F(\mathbf{x}) = \frac{E_1 A^{3/2}}{M_{cr}}, \tag{1}$$

where $\mathbf{x}$ is the vector of the design variables, A is the cross-sectional area, E_1 is the Young's modulus in the x_1 direction and M_{cr} is the critical moment given by

$$M_{cr} = \lambda M_0^{ref}, \tag{2}$$

being M_0^{ref} a reference moment, which is function of the current loading, and λ a dimensionless global load parameter. Multiplying λ by the current loading, the critical load is obtained and the global elastic instability of the structure is achieved.

The components of $\mathbf{x}$ are defined as: the fiber orientation of the kth layer θ_k, the dimensions of the cross-section, b and h, the thickness of each layer t_c and the number of layers of the laminate n. The magnitudes t_c and n define the total wall thickness t (see Fig. 1).

The structural constraints take into account the strength of laminate, the global and local stability of the beam and the maximum allowed displacement. The structure must also verify the condition of thin-walled beams. In addition, it is established that the area of the cross-section does not overcome a maximum value (A_{max}) according to the requirements of a preliminary design. In summary, the complete optimization problem is written as follows

$$\begin{aligned} &\min_{\mathbf{x}=(h,b,t_c,n,\theta_k)} \quad \frac{E_1 A(\mathbf{x})^{3/2}}{M_{cr}(\mathbf{x})}, \\ &\text{subject to} \\ &R_{min}(\mathbf{x}) > 1, \quad \lambda(\mathbf{x}) > 1, \quad \delta(\mathbf{x}) \le \delta_{máx}, \quad \lambda_L(\mathbf{x}) > 1, \\ &A(\mathbf{x}) \le A_{max}, \quad min(b/t, h/t) \quad \ge 10, \\ &\mathbf{x}^{\mathbf{L}} \le \mathbf{x} \le \mathbf{x}^{\mathbf{U}}, \quad \theta_k = (0^o, 90^o), \end{aligned} \tag{3}$$

where λ_L is the local load parameter and the ratios b/t and h/t represent the slenderness of the beam. The displacement module (δ) is defined as the square root of the sum of squared displacement and must be less than the maximum displacement allowed. In this case, we considered that limit as a standard value set to 2.5 per thousand of the beam length ($L/400$). R_{min} is the lowest safety factor, which is calculated at the points shown in Fig. 2. This safety factor is obtained according to the Tsai-Wu failure criterion [19]. To calculate R_{min}, the stresses are needed. These are calculated employing the beam model presented in the next section.

3. Composite thin-walled beam model

A theoretical model is developed to find displacements, stresses and global buckling loads which will be used to solve the optimization problem. This model represents an extension of the work in reference [11], in order to account an arbitrary state of initial stresses. The effect of shear deformability due to both bending and non-uniform warping is taken into account and the Hellinger-Reissner Principle is employed. Composite thin-walled beams of closed and open cross-section subjected to any boundary condition are considered. This theory is valid only for FRP materials with orthotropic lamination (symmetric balanced, orthotropic and cross-ply laminates).

3.1. Displacement and strain fields

In the Fig. 3, B is a generic point in the middle line of the wall. Two reference points are employed: the point C, coincident with

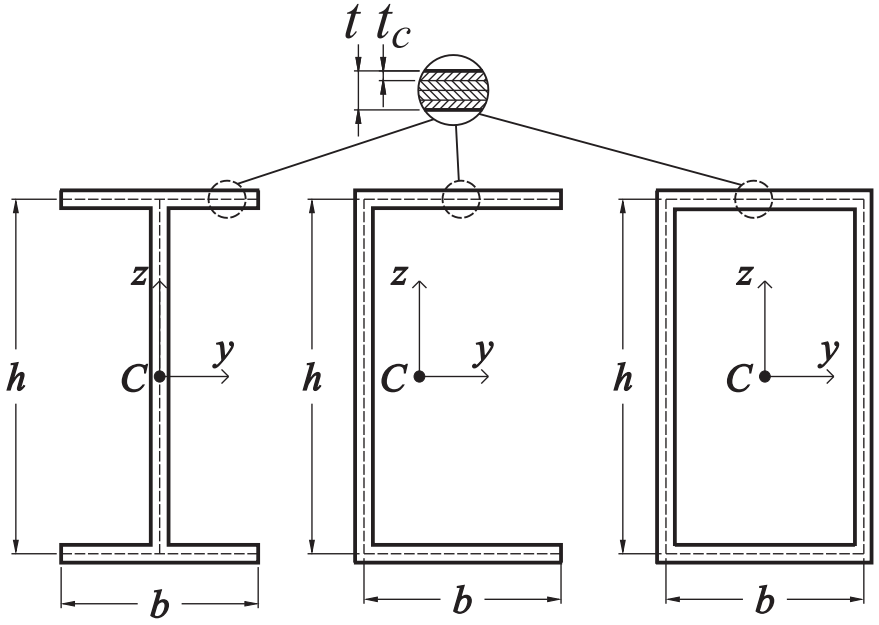

Fig. 1. Detail of the dimensions of I, C and box profiles.

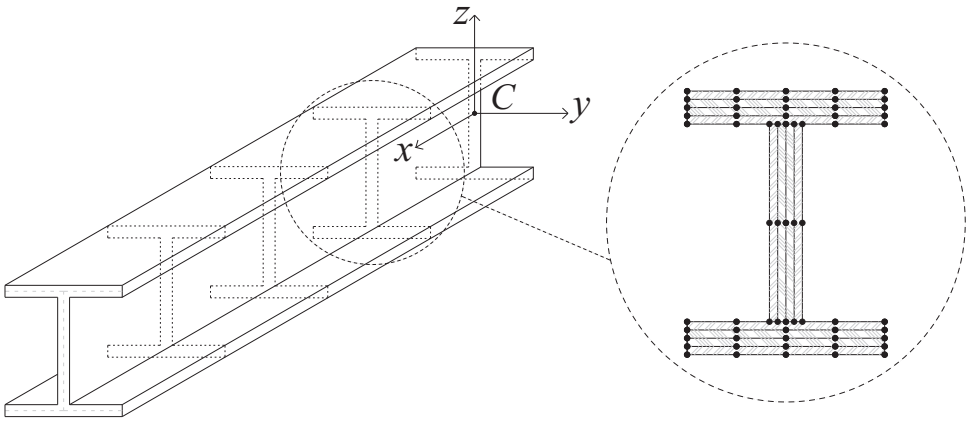

Fig. 2. Points where the stresses are calculated for an I-beam.

the centroid of the cross-section, and the point O, coincident with the shear center of the corresponding isotropic cross-section, according to the Vlasov theory [20]. Magnitudes V, L and S represent the volume, the length and the perimeter of middle line, respectively.

The Cartesian coordinates corresponding to a point on the cross section are

$$y(s,n)=\bar{y}-y_0, \qquad z(s,n)=\bar{z}-z_0,$$
$$y(s,n)=Y-n\frac{dZ}{ds}, \qquad z(s,n)=Z+n\frac{dY}{ds}, \tag{4}$$

where Y and Z are the coordinates corresponding to points lying on this middle line.

The present thin-walled beam theory is based on the following two principal hypotheses: (1) the cross-section contour is rigid in its own plane, although it is free to warp out of it, and (2) the torsional warping distribution is assumed to be given by the Saint-Venant function corresponding to the cross-section considered as isotropic. According to these assumptions, the displacement field is assumed to be

$$u_x=u-y\theta_z-z\theta_y-\omega\theta_x', \qquad u_y=v-\bar{z}\phi_x, \quad u_z=w+\bar{y}\phi_x,$$
$$u_x^{NL}=\frac{1}{2}\left(z\phi_x\theta_z-y\phi_x\theta_y\right),$$
$$u_y^{NL}=\frac{y}{2}\left(\phi_x^2+\theta_z^2\right)-\frac{z}{2}\theta_z\theta_y, \qquad u_z^{NL}=\frac{z}{2}\left(\phi_x^2+\theta_y^2\right)-\frac{y}{2}\theta_z\theta_y, \tag{5}$$

where ω is the warping function (see [11]), u, v and w are the displacements in x, y and z directions, respectively, θ_y and θ_z are bending twists, ϕ_x is the torsional twist and θ_x is the warping variable (see Fig. 3). The displacement field can also be expressed in terms of the intrinsic system (B: x, s, n) as

$$U^L=u_x, \qquad V^L=u_y\frac{dY}{ds}+u_z\frac{dZ}{ds}, \qquad W^L=-u_y\frac{dZ}{ds}+u_z\frac{dY}{ds},$$
$$U^{NL}=u_x^{NL}, \quad V^{NL}=u_y^{NL}\frac{dY}{ds}+u_z^{NL}\frac{dZ}{ds}, \quad W^{NL}=-u_y^{NL}\frac{dZ}{ds}+u_z^{NL}\frac{dY}{ds},$$
$$\Phi_x=-\frac{\partial u_x}{\partial n}, \quad \Phi_s=\frac{\partial}{\partial n}\left(u_y\frac{dY}{ds}+u_z\frac{dZ}{ds}\right), \tag{6}$$

where U, V and W are the shell displacement in x, s and n directions, respectively, and Φ_x and Φ_s are the bending twists with respect to s and n directions, respectively.

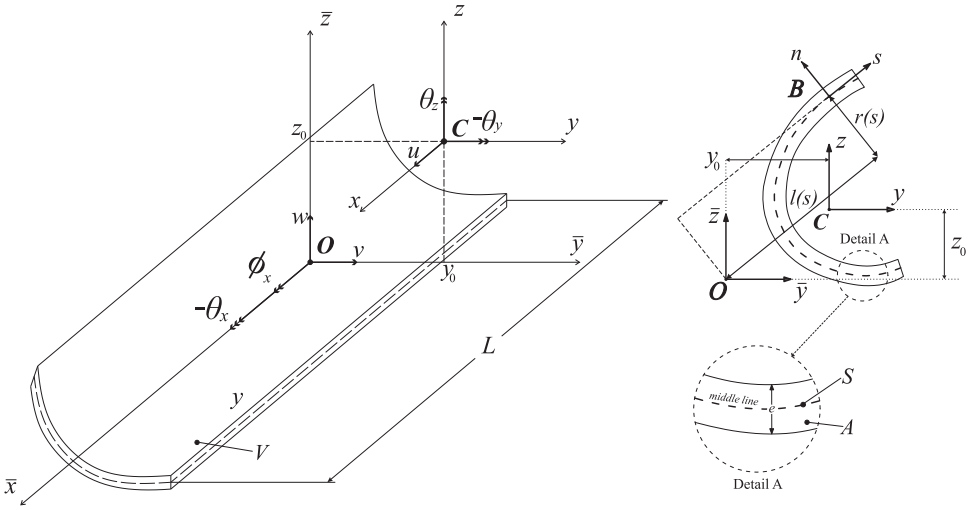

Fig. 3. Geometrical entities of the cross-section, coordinate systems and displacement field.

Strain components of first order due to linear and non-linear displacement and strain components of second order due to linear displacement are considered. Therefore, the components of the Green-Lagrange tensor are expressed in the intrinsic system by means of the following expressions

$$\varepsilon_{xx} = \frac{\partial U^L}{\partial x}, \quad \varepsilon_{xs} = \frac{1}{2}\left(\frac{\partial U^L}{\partial s} + \frac{\partial V^L}{\partial x}\right), \quad \varepsilon_{xn} = \frac{1}{2}\left(\frac{\partial U^L}{\partial n} + \frac{\partial W^L}{\partial x}\right),$$
$$\eta_{xx} = \frac{\partial U^{NL}}{\partial x} + \frac{1}{2}\left[\left(\frac{\partial U^L}{\partial x}\right)^2 + \left(\frac{\partial V^L}{\partial x}\right)^2 + \left(\frac{\partial W^L}{\partial x}\right)^2\right],$$
$$\eta_{xs} = \frac{1}{2}\left(\frac{\partial U^{NL}}{\partial s} + \frac{\partial V^{NL}}{\partial x}\right) + \frac{1}{2}\left(\frac{\partial U^L}{\partial s}\frac{\partial U^L}{\partial x} + \frac{\partial V^L}{\partial s}\frac{\partial V^L}{\partial x} + \frac{\partial W^L}{\partial s}\frac{\partial W^L}{\partial x}\right),$$
$$\eta_{xn} = \frac{1}{2}\left(\frac{\partial U^{NL}}{\partial n} + \frac{\partial W^{NL}}{\partial x}\right) + \frac{1}{2}\left(\frac{\partial U^L}{\partial n}\frac{\partial U^L}{\partial x} + \frac{\partial V^L}{\partial n}\frac{\partial V^L}{\partial x} + \frac{\partial W^L}{\partial n}\frac{\partial W^L}{\partial x}\right). \tag{7}$$

Also, the linear strain components can be expressed in terms of membranal strain and curvatures follows

$$\varepsilon_{xx} = \varepsilon_{xx}^L + n\kappa_{xx}^L, \quad \gamma_{xs} = \gamma_{xs}^L + n\kappa_{xs}^L, \quad \gamma_{xn} = \gamma_{xn}^L, \tag{8}$$

where

$$\epsilon_{xx}^L = u' - Y\theta_z' - Z\theta_y' - \omega_p\theta_x', \qquad \kappa_{xx}^L = \frac{dZ}{ds}\theta_z' - \frac{dY}{ds}\theta_y' - l\theta_x',$$
$$\gamma_{xs}^L = \frac{dY}{ds}(v' - \theta_z) + \frac{dZ}{ds}(w' - \theta_y) + (r + \psi)\theta_x - r\phi_x', \qquad \kappa_{xs}^L = -(\theta_x + \phi_x'),$$
$$\gamma_{xn}^L = -\frac{dZ}{ds}(v' - \theta_z) + \frac{dY}{ds}(w' - \theta_y) + l(\phi_x' - \theta_x). \tag{9}$$

In above expressions $(\bullet)'$ denotes derivation with respect to x.

3.2. One-dimensional variational equation of equilibrium

The principle of Hellinger-Reissner comprises two expressions [21]. One represents the principle of Virtual Work while the other is interpreted as a variational representation of the constitutive equations expressed in terms of the linear strain components. Both equations are written as

$$L_S + L_S^0 + L_T + L_T^0 + L_F + L_F^0 = 0, \tag{10}$$

$$\int\int\left[\left(\varepsilon_{xx}^L - \frac{N_{xx}}{A_{11}}\right)\delta N_{xx} + \left(\gamma_{xs}^L - \frac{N_{xs}}{A_{66}}\right)\delta N_{xs} + \left(\kappa_{xs}^L - \frac{M_{xs}}{D_{66}}\right)\delta M_{xs}\right] ds\, dx$$
$$+ \int\int\left[\left(\kappa_{xx}^L - \frac{M_{xx}}{D_{11}}\right)\delta M_{xx} + \left(\gamma_{xn}^L - \frac{N_{xn}}{A_{55}^{(H)}}\right)\delta N_{xn}\right] ds\, dx = 0, \tag{11}$$

where A_{ij} and D_{ij} are tensile and bending stiffness of a laminate. L_S and L_S^0 are the virtual work of the first order strain due to incremental stress and initial stress, respectively. L_F and $L_F^0$are the virtual work of the linear and non-linear displacements due to current and initial volumetric forces, respectively. L_T and L_T^0 are the virtual work of the linear and non-linear displacements due to current and initial surface forces, respectively. Finally, L_R is the virtual work of the displacements due to inertial forces. Integrating with respect to s, the one-dimensional expressions are obtained as

$$L_S = \int_0^L \left(N\delta u' - M_y\delta\theta_y' - M_z\delta\theta_z' - B\delta\theta_x' + Q_y\delta(v' - \theta_z) + Q_z\delta(w' - \theta_y) + T_w\delta(\phi_x' - \theta_x) + T_{sv}\delta\phi_x'\right)dx, \tag{12}$$

$$L_S^0 = \int_0^L \frac{N^0}{2}\left\{\delta v'^2 + \delta w'^2 + \delta u'^2 - 2z_0\delta v'\phi_x' - 2y_0\delta w'\phi_x'\right\}dx +$$
$$\int_0^L \frac{M_y^0}{2}\left(\delta\phi_x'\theta_z + \delta\phi_x\theta_z' - 2\delta u'\theta_y' - 2\delta\phi_x'v'\right)dx +$$
$$\int_0^L \frac{M_z^0}{2}\left[2\delta w'\phi_x' - \delta\left(\theta_y\phi_x\right)' - 2\delta u'\theta_z'\right]dx - \int_0^L B^0\delta u'\theta_x' dx +$$
$$\int_0^L Q_y^0\left(\delta\phi_x w' - \delta u'\theta_z - \frac{\delta\phi_x\theta_y}{2}\right)dx - \int_0^L T_w^0\delta\theta_x u' dx +$$
$$\int_0^L Q_z^0\left(\frac{\delta\phi_x\theta_z}{2} - \delta\phi_x v' - \delta u'\theta_y\right)dx + \int_0^L \frac{M_x^0}{2}\left(\delta\theta_y\theta_z' - \delta\theta_y'\theta_z\right)dx, \tag{13}$$

$$L_F + L_F^0 = -\int_0^L \left(q_x\delta u - m_z\delta\theta_z - m_y\delta\theta_y - b\delta\theta_x + q_y\delta v + q_z\delta w + m_x\delta\phi_x\right)dx$$
$$- \int_0^L \left(q_2^0\delta\theta_z + q_3^0\delta\theta_y + q_4^0\delta\phi_x\right)dx, \tag{14}$$

$$L_T + L_T^0 = -\left(\bar{N}\delta u - \bar{M}_z\delta\theta_z - \bar{M}_y\delta\theta_y + \bar{B}\delta\theta_x + \bar{Q}_y\delta v + \bar{Q}_z\delta w + \bar{M}_x\delta\phi_x\right)_{x=0}^{x=L}$$
$$- \left(\bar{N}_2^0\delta\theta_z + \bar{N}_3^0\delta\theta_y + \bar{N}_4^0\delta\phi_x\right)_{x=0}^{x=L}, \tag{15}$$

where $(\bullet^0)$ refers to initial stress state. N, Q_y, Q_z, M_y, M_z, B, T_w and T_{sv} are the generalized beam forces, N^0, M_y^0, M_z^0, B^0, Q_y^0, Q_z^0, T_w^0 and M_x^0 are the initial beam stress resultants, q_x, q_y and q_z are the applied forces per unit length in the directions x, y and z, respectively, m_x, m_y and m_z are the applied couples per unit length about the directions x, y and z, respectively, b is the applied bimoment per unit length, q_2^0, q_3^0 and q_4^0 are the volume initial forces (see Appendix A). $\bar{N}$, $\bar{M}_z$, $\bar{M}_y$, $\bar{B}$, $\bar{Q}_y$, $\bar{Q}_z$ and $\bar{M}_x$ are the external generalized forces acting at the ends, $\bar{N}_2^0$, $\bar{N}_3^0$ and $\bar{N}_4^0$ are the surface initial forces (see Appendix A). The beam forces have been defined in terms of the shell stress resultants as

$$N = \int_S N_{xx}\, ds, \quad M_y = \int_S\left(N_{xx}Z + M_{xx}\frac{dY}{ds}\right)ds, \quad M_z = \int_S N_{xx}Y - M_{xx}\frac{dZ}{ds}ds,$$
$$Q_y = \int_S\left(N_{xs}\frac{dY}{ds} - N_{xn}\frac{dZ}{ds}\right)ds, \quad Q_z = \int_S\left(N_{xs}\frac{dZ}{ds} + N_{xn}\frac{dY}{ds}\right)ds,$$
$$B = \int_S\left(N_{xx}\omega_p + M_{xx}l\right)ds, \quad M_x = T_w + T_{sv},$$
$$T_w = \int_S\left[-N_{xs}(r + \psi) + M_{xs} + N_{xn}l\right]ds, \quad T_{sv} = \int_S\left(N_{xs}\psi - 2M_{xs}\right)ds, \tag{16}$$

where the shell stress resultants are expressed in terms of the stresses as

$$N_{xx} = \int_{-t/2}^{t/2}\sigma_{xx}\, dn, \quad M_{xx} = \int_{-t/2}^{t/2}(\sigma_{xx}n)\, dn,$$
$$N_{xs} = \int_{-t/2}^{t/2}\sigma_{xs}\, dn, \quad M_{xs} = \int_{-t/2}^{t/2}(\sigma_{xs}n)\, dn, \quad N_{xn} = \int_{-t/2}^{t/2}\sigma_{xn}\, dn. \tag{17}$$

The initial beam stress resultants are defined analogously to the beam forces of Eq. (16), but related to the initial stresses.

3.3. Constitutive equations

For orthotropic and symmetric laminates, the constitutive equations in terms of the shell stress resultants are

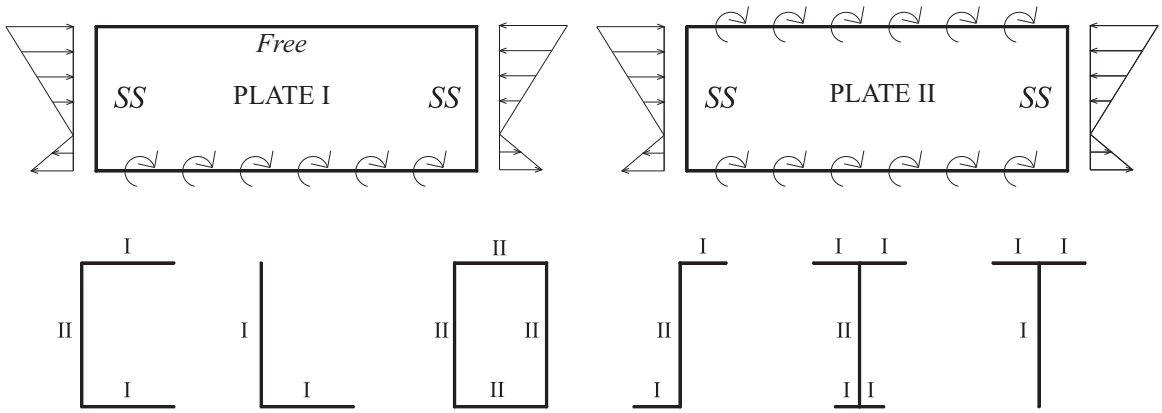

Fig. 4. Local buckling analysis of FRP beams.

$$\begin{Bmatrix} N_{xx} \\ N_{xs} \\ N_{xn} \\ M_{xx} \\ M_{xs} \end{Bmatrix} = \begin{bmatrix} \bar{A}_{11} & 0 & 0 & 0 & 0 \\ 0 & \bar{A}_{66} & 0 & 0 & 0 \\ 0 & 0 & \bar{A}_{55}^{(H)} & 0 & 0 \\ 0 & 0 & 0 & \bar{D}_{11} & \bar{D}_{16} \\ 0 & 0 & 0 & \bar{D}_{16} & \bar{D}_{66} \end{bmatrix} \begin{Bmatrix} \varepsilon_{xx}^{L} \\ \gamma_{xs}^{L} \\ \gamma_{xn}^{L} \\ \kappa_{xx}^{L} \\ \kappa_{xs}^{L} \end{Bmatrix}, \tag{18}$$

where $\bar{A}_{ij}$ and $\bar{D}_{ij}$ are the modified stiffness coefficients defined as

$$\bar{A}_{11} = A_{11} - \frac{A_{12}^2}{A_{22}}, \quad \bar{A}_{66} = A_{66}, \quad \bar{A}_{55}^{(H)} = A_{55}^{(H)} - \frac{\left(A_{45}^{(H)}\right)^2}{A_{44}^{(H)}},$$
$$\bar{D}_{11} = D_{11} - \frac{D_{12}^2}{D_{22}}, \quad \bar{D}_{66} = D_{66} - \frac{D_{26}^2}{D_{22}}, \quad \bar{D}_{16} = D_{16} - \frac{D_{26}D_{12}}{D_{22}}. \tag{19}$$

The field of the shell stress resultants is proposed to satisfy Eq. (18) and the shell equilibrium equations (see [11]). Thus, such field is written as

$$N_{xx} = t\left[\frac{N}{A} + \frac{M_y}{I_y}Z + \frac{M_z}{I_z}Y + \frac{B}{C_w}\omega_P\right],$$
$$M_{xx} = \frac{t^3}{12}\left[\frac{M_y}{I_y}\frac{dY}{ds} - \frac{M_z}{I_z}\frac{dZ}{ds} - \frac{B}{C_w}I\right], \quad M_{xs} = -\frac{t^3}{6J}T_{sv},$$
$$N_{xs} = -t\left[\frac{Q_z}{I_y}\lambda_y + \frac{Q_y}{I_z}\lambda_z + \frac{T_w}{C_w}\lambda_\omega\right] + \frac{t\psi}{J}T_{sv},$$
$$N_{xn} = \frac{t^3}{12}\left[\frac{Q_z}{I_y}\frac{dY}{ds} - \frac{Q_y}{I_z}\frac{dZ}{ds} - \frac{T_w}{C_w}I\right], \tag{20}$$

where

$$\lambda_y(s) = \int_0^s Z ds + \frac{\chi}{S}\oint\left(\int_0^s Z ds\right) ds,$$
$$\lambda_z(s) = \int_0^s Y ds + \frac{\chi}{S}\oint\left(\int_0^s Y ds\right) ds,$$
$$\lambda_\omega(s) = \int_0^s \omega_P ds + \frac{\chi}{S}\oint\left(\int_0^s \omega_P ds\right) ds, \tag{21}$$

being χ 0 or 1 whether the cross section is open or closed, respectively. Furthermore, A, I_y, I_z, I_{yz}, $I_{y\omega}$, $I_{z\omega}$, C_w and J are the cross-sectional constants defined as

$$A = \int_A dA, \quad I_y = \int_A Z^2 dA, \quad I_z = \int_A Y^2 dA, \quad I_{yz} = \int_A YZ dA,$$
$$I_{y\omega} = \int_A Z\omega_p dA, \quad I_{z\omega} = \int_A Y\omega_p dA, \quad C_w = \int_A \omega_p^2 dA, \quad J = \frac{1}{3}\int_S e^3 ds. \tag{22}$$

The constitutive equations in terms of the beam forces are obtained by replacing the field of the shell stress resultants (20) into the functional (11). Integrating with respect to s and taking variations with respect to the beam forces, the following constitutive equations are found

$$\mathbf{Q} = \mathbf{J}\cdot\boldsymbol{\Delta}, \tag{23}$$

where $\mathbf{Q}$ is the vector of the beam forces, $\boldsymbol{\Delta}$ is the vector of the generalized strains and $\mathbf{J}$ is the constitutive matrix. All of which are defined as

$$\mathbf{Q} = \left\{N, M_y, M_z, B, Q_y, Q_z, T_w, T_{sv}\right\}^T, \tag{24}$$

$$\boldsymbol{\Delta} = \left\{u', -\theta_y', -\theta_z', -\theta_x', v' - \theta_z, w' - \theta_y, \phi_x' - \theta_x, \phi_x'\right\}^T, \tag{25}$$

$$\mathbf{J} = \begin{bmatrix} \hat{EA} & 0 & 0 & 0 & 0 & 0 & 0 & 0 \\ & \hat{EI}_y & 0 & 0 & 0 & 0 & 0 & 0 \\ & & \hat{EI}_z & 0 & 0 & 0 & 0 & 0 \\ & & & \hat{EC}_w & 0 & 0 & 0 & 0 \\ & & & & \hat{GS}_y & \hat{GS}_{yz} & \hat{GS}_{y\omega} & 0 \\ & & sym & & & \hat{GS}_z & \hat{GS}_{z\omega} & 0 \\ & & & & & & \hat{GS}_\omega & 0 \\ & & & & & & & \hat{GJ} \end{bmatrix}. \tag{26}$$

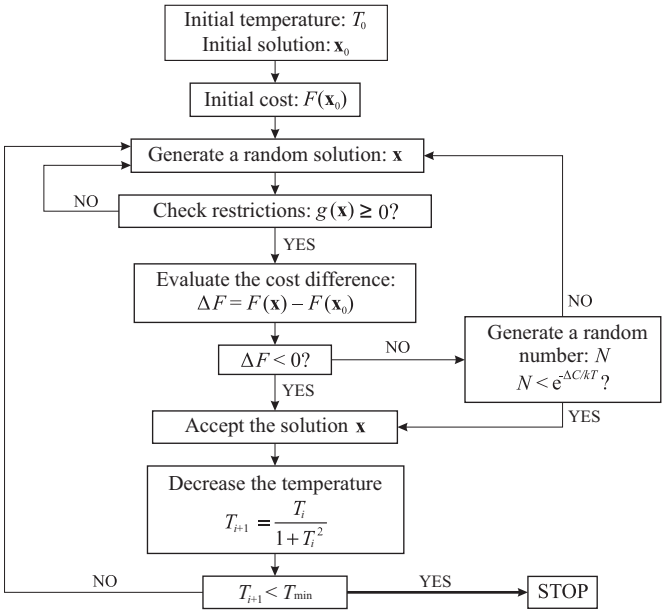

Fig. 5. Flowchart of Simulated Annealing algorithm.

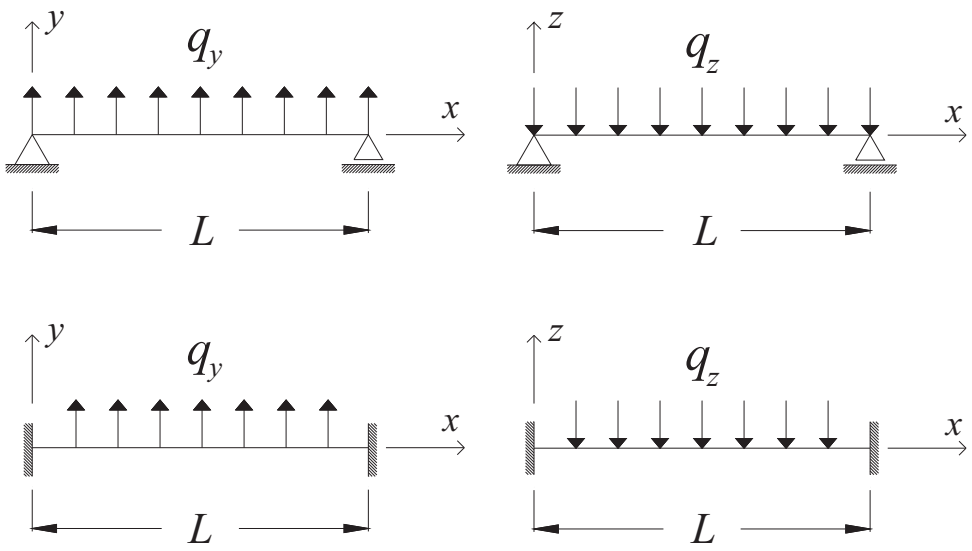

Fig. 6. Preliminary requirements of the designs.

The elements of the constitutive matrix are

$$\hat{EA} = \bar{A}_{11}\int_S ds, \quad \hat{EI}_y = \bar{A}_{11}\int_S Z^2 ds + \bar{D}_{11}\int_S \left(\frac{dY}{ds}\right)^2 ds,$$

$$\hat{EI}_z = \bar{A}_{11}\int_S Y^2 ds + \bar{D}_{11}\int_S \left(\frac{dZ}{ds}\right)^2 ds, \quad \hat{EC}_w = \bar{A}_{11}\int_S \omega_p^2 ds + \bar{D}_{11}\int_S l^2 ds, \tag{27}$$

$$\begin{bmatrix} \hat{GS}_y & \hat{GS}_{yz} & \hat{GS}_{y\omega} \\ & \hat{GS}_z & \hat{GS}_{z\omega} \\ sim & & \hat{GS}_\omega \end{bmatrix} = \left(\frac{t}{\bar{A}_{66}} \begin{bmatrix} \int_S \left(\frac{\lambda_z}{I_z}\right)^2 ds & \int_S \frac{\lambda_z \lambda_y}{I_y I_z} ds & -\int_S \frac{\lambda_z \lambda_\omega}{I_z C_w} ds \\ & \int_S \left(\frac{\lambda_y}{I_y}\right)^2 ds & -\int_S \frac{\lambda_\omega \lambda_y}{I_y C_w} ds \\ sym & & \int_S \left(\frac{\lambda_\omega}{C_w}\right)^2 ds \end{bmatrix} \right.$$

$$\left. + \frac{t^4}{144\bar{A}_{55}^{(H)}} \begin{bmatrix} \int_S \left(\frac{dZ}{ds}\frac{1}{I_z}\right)^2 ds & \int_S \left(\frac{dY}{ds}\frac{dZ}{ds}\frac{1}{I_y I_z}\right) ds & -\int_S \left(\frac{\partial \omega_p}{\partial n}\frac{dZ}{ds}\frac{1}{I_z C_w}\right) ds \\ & \int_S \left(\frac{dY}{ds}\frac{1}{I_y}\right)^2 ds & -\int_S \left(\frac{dY}{ds}\frac{\partial \omega_p}{\partial n}\frac{1}{I_y C_w}\right) ds \\ sym & & \int_S \left(\frac{\partial \omega_p}{\partial n}\frac{1}{C_w}\right)^2 ds \end{bmatrix} \right]^{-1}, \tag{28}$$

$$\hat{GJ} = \bar{A}_{66}\int_S \psi^2 ds + \bar{A}_{55}^{(H)}\int_S l^2 ds + 4\bar{D}_{66}\int_S ds. \tag{29}$$

4. Solution methods

4.1. Finite element analysis

In order to solve the static and instability problems, a non-locking finite element based on the present theory is employed. This finite element has two nodes with seven degrees-of-freedom per node and employs third-degree polynomial shape functions [12].

For the case of static and buckling analysis, the general finite element equation leads to the following eigenvalue problem

$$(\mathbf{K} + \lambda\, \mathbf{K_G})\mathbf{W}^* = 0, \tag{30}$$

where $\mathbf{K}$ and $\mathbf{K_G}$ are global matrices of elastic stiffness and geometric stiffness, respectively; whereas $\mathbf{W}^*$ is the global incremental displacement vector.

In order to obtain the initial stresses, the following finite element form of the self-equilibrium condition of initial stresses and initial volume and surface forces is employed

$$\mathbf{K}^0\mathbf{W}^0 = \mathbf{P}^0, \tag{31}$$

where $\mathbf{K^0}$, $\mathbf{W^0}$ and $\mathbf{P^0}$ are the global matrix of initial elastic stiffness, the global vector of initial nodal displacements and the

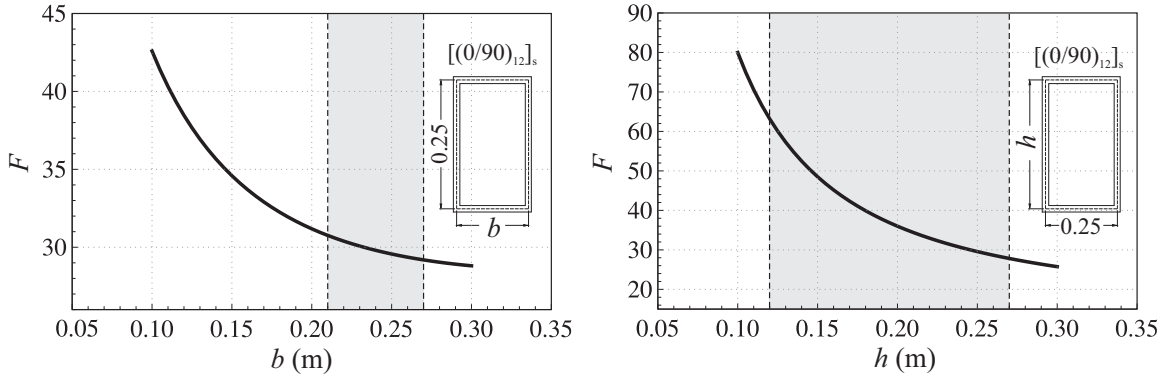

Fig. 7. Dependence of the objective function F with respect to the design variables b and h. n and θ_k fixed.

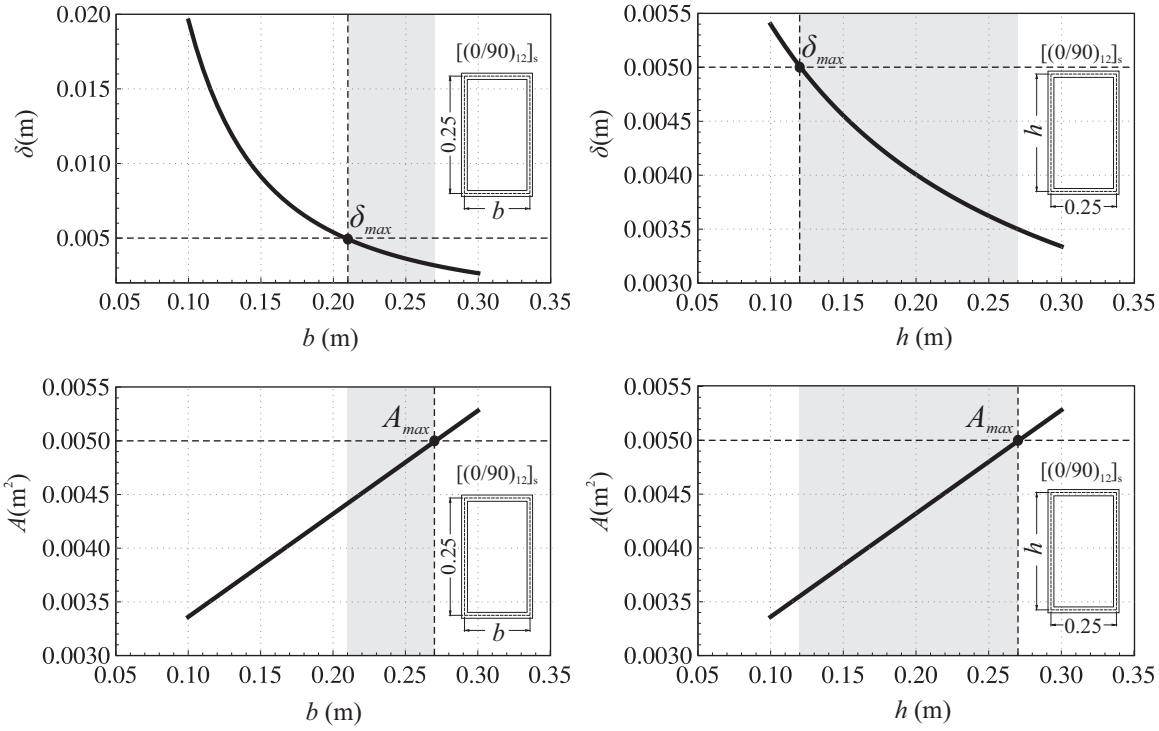

Fig. 8. Active restrictions as functions of b and h.

global vector of initial volume and surface forces, respectively. Once $\mathbf{W^0}$ is found, the global matrix of geometric stiffness can be determined. This allows calculations of global buckling loads and the vibration behavior under the presence of initial stresses.

4.2. Local buckling

The local buckling analysis is performed by modeling the wall segments as long plates, assuming that the common edges of two or more plates remain straight. In order to calculate the buckling load, the wall segments are regarded as individual plates elastically restrained by their adjacent walls [22] (see Fig. 4).

To analyze the local buckling, a procedure similar to the one developed in [17] is employed. Their expressions of the buckling loads of long composite orthotropic plates are employed to determinate the buckling loads of the web and flanges. First, the edges of each pair of segments are regarded as simply supported and two buckling loads are obtained. These loads are compared to check which segment buckles first. Finally, the buckling load of this segment is found, assuming restrained edges by taking into account the stiffness of the adjacent wall.

4.3. Simulated Annealing algorithm

Simulated Annealing algorithm [23] is based on an iterative procedure, in which a random point is chosen and updated until a convergence criterion is fulfilled (see Fig. 5). For each iteration, a random point is generated in the nearness of the current configuration. If this point produces a smaller value of the cost compared to that of the current record, the point is accepted and replaces the old one. On the other hand, if the new cost produces a bigger value, the acceptability of the point is determined according to the probability of Boltzmann distribution. This probability depends on a parameter T, called 'temperature'. The convergence of Simulated Annealing is assured when the temperature tends towards zero. At initial stages of the algorithm (at high temperatures), the probability of taking worse designs is higher. When the temperature is decreases, this probability becomes smaller so that in the final stages of the algorithm, solutions producing high costs are almost not accepted. The cooling scheme proposed in [24] is employed since it minimizes computational efforts compared with the classic geometric scheme. This scheme is given by

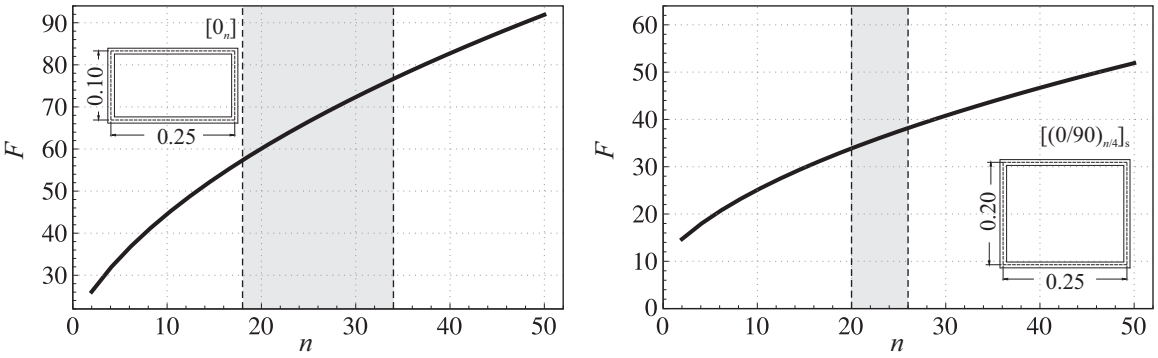

Fig. 9. Dependence of the objective function F with respect to the design variable n. b, h and θ_k fixed.

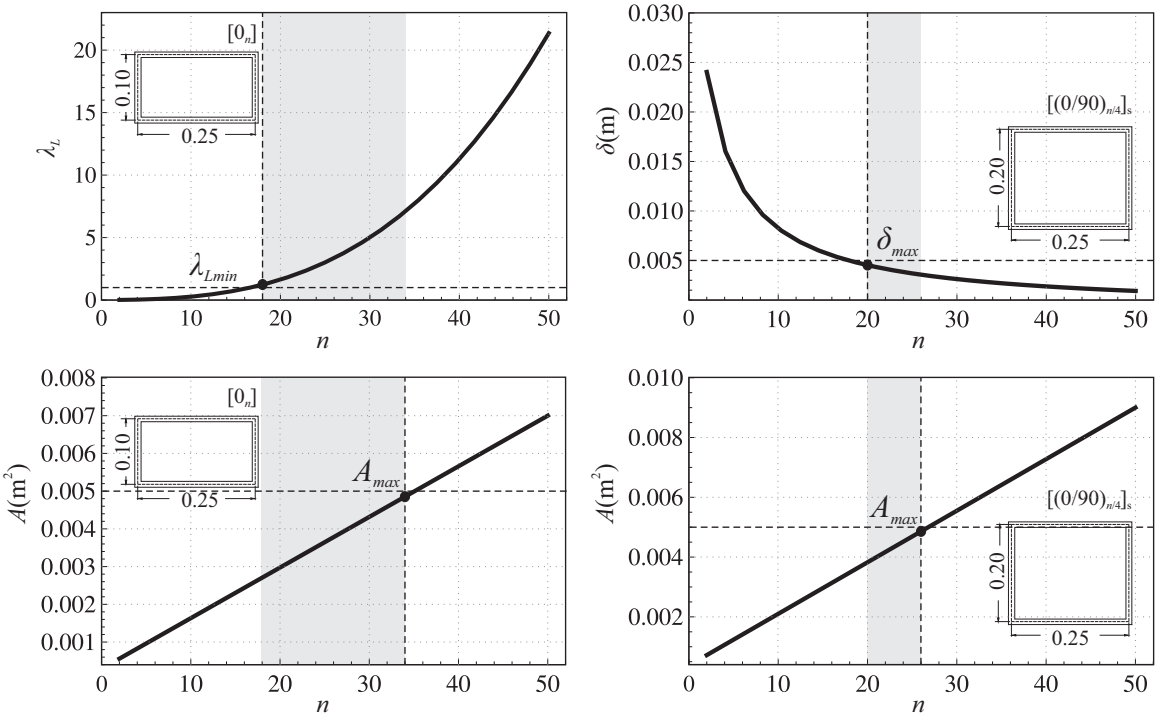

Fig. 10. Active restrictions as functions of n.

Table 1
Comparison between optimal and standard (non-optimal) solutions, for SS beams.

Solution	Load [kN/m]	Cross-section	Width b [mm]	Height h [mm]	Number of layers n	Lay-up	λ	A [mm^2]	Cost
Optimal	$q_y=-50$	Box	230	290	24	$[(0/90)_{12}]_s$	94	4992	26.92
Solution 1			220	220	24	$[(0/90)_{12}]_s$	59	4224	33.74
Optimal	$q_z=-50$	Box	290	230	24	$[(0/90)_{12}]_s$	94	4992	26.92
Solution 2			200	300	24	$[(0/90)_{12}]_s$	68	4800	35.48

$$T_{i+1} = \frac{T_i}{1 + T_i^2}. \tag{32}$$

The main characteristic of the method is that it achieves an absolute minimum or a good relative minimum for the objective function. Nevertheless, there exists a necessary (although insufficient) condition, so that the optimization process does not get trapped in a local minimum. For this reason, the initial temperature T_0 must be sufficiently high so that, at the end of the first stage, all the configurations can be obtained with the same probability. A suitable expression of T_0 is used in this work, given by [25].

$$T_0 = r \cdot \Delta F_{\max}, \tag{33}$$

where $r > 1$ and $\Delta F_{\max}$ is the maximum value of the cost variation.

5. Results and discussion

5.1. Overview

Clamped-clamped (CC) and simply supported (SS) box, C and I-beams subjected to distributed loads in y and z directions are designed. Fig. 6 shows the pre-established requirements of the designs. The magnitude of the load is 50 kN/m and the maximum area allowed is 0.005 m^2. The material used is Graphite/Epoxy T300/5208, whose properties are $E_1=181$ GPa, $E_2=10.3$ GPa, $G_{12}=7.17$ GPa, $\upsilon_{12}=0.28$, and strengths are given by $s_1^+=1500$ MPa, $s_1^-=1500$ MPa, $s_2^+=40$ MPa, $s_2^-=246$ MPa, $s_{12}=68$ MPa. The thickness of each layer is considered to be constant ($t_s=0.2$ mm). The length of the beam (L) is 2 m. The domain of the design variables is given by $h\in[0.1{:}0.01{:}0.3]$ m, $b\in[0.1{:}0.01{:}0.3]$ m, $n\in[1{:}1{:}50]$ and $\theta_k\in(0, 90)$ such the possible laminates are $[0_n]$, $[90_n]$ or $[(0/90)_{n/2}]_s$.

5.2. Parametric analysis of the optimization problem

Before solving the optimization problem, a parametric analysis is performed in order to understand the behavior of the objective function and the restrictions, in terms of the design indicators. This study provides more information about the problem to solve. Fig. 7 shows the dependence of the objective function with respect to the design variables b and h, while the other variables (n and θ_k) remain fixed. The shaded zone indicates the feasible area, i.e. the zone where the restrictions are fulfilled. This area is bounded by the active restrictions, whose dependence on b and h is presented in Fig. 8. For both dependences, the lower bound is defined by the maximum displacement and the upper bound is imposed by the restriction of maximum area.

Figs. 9 and 10 show respectively the objective function and the active restrictions plotted as functions of the number of layers of the laminate, n. It can be seen from Fig. 10 that for $[0_n]$ laminate,

Table 2
Optimal solutions for CC beams.

Load [kN/m]	Cross-section	Optimal width b [mm]	Optimal height h [mm]	Optimal number of layers n	Optimal lay-up	λ	A [mm^2]	Minimum cost	Active restriction
q_y=50	Box	260	300	20	$[(0/90)_{10}]_s$	210	4480	15.47	Local buckling Maximum area
	I	180	280	39	$[0_{39}]$	199	4992	19.19	Local buckling Maximum area
	C	150	300	41	$[0_{41}]$	78	4920	47.89	Local buckling Maximum area
q_z=−50	Box	300	300	20	$[(0/90)_{10}]_s$	235	4800	15.34	Local buckling Limits of the ranges
	I	300	300	25	$[0_{25}]$	225	4500	13.95	Local buckling Limits of the ranges
	C	150	280	43	$[0_{43}]$	73	4988	33.58	Local buckling Maximum area

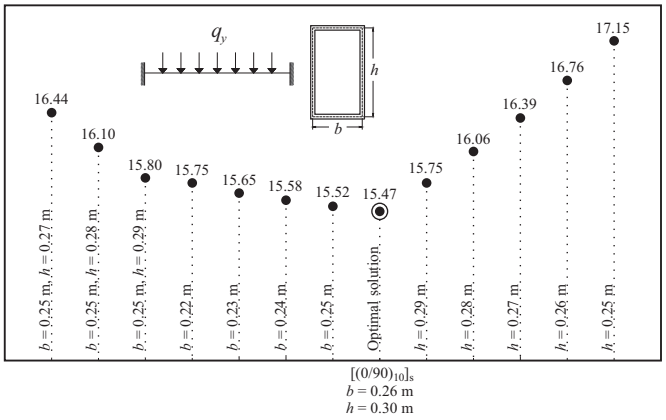

Fig. 11. Objective function for the optimal solution and several standard solutions.

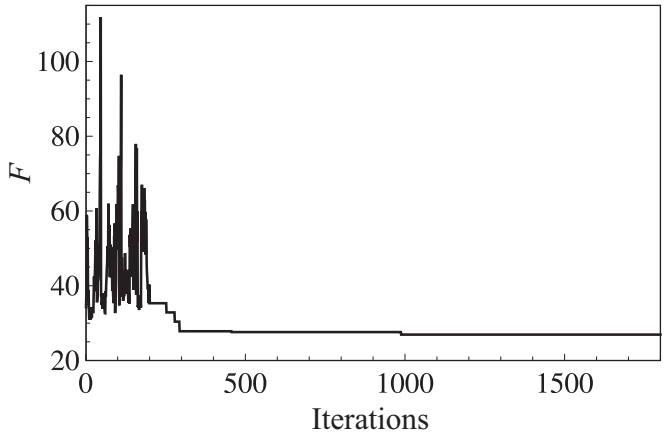

Fig. 12. Convergence of the SA algorithm for the design of a SS box-beam under q_z loading.

the lower bound is delimited by the local buckling restriction instead of maximum displacement.

5.3. Implementation of the design scheme

The optimal design proposed in Eq. (3) is applied in order to find the optimal characteristics of composite thin-walled beams. Tables 1 and 2 show the results obtained for the cases studied (see Fig. 6). The optimal cross-sections which minimize the objective function are found, reducing the weight and increasing the resistance to global buckling. Table 1 show results for SS beams under uniformly distributed load of intensity q_y and q_z. It can be seen that the same optimal solution is obtained for both loads in terms of the number of layers and the laminate stacking. Comparing both loading conditions, one can see that an appropriate resistance to global buckling and the minimum cross-sectional area are reached only by interchanging the dimensions b and h. The optimal solutions obtained are also compared with other non-optimal solutions that satisfy the conditions of the design (Solutions 1 and 2). Of course, these solutions correspond to higher values of the objective function, for both loading conditions. The non-optimal solutions produce a lower weight, but at the expense of a lower buckling strength. In these particular cases, the buckling strength is not the maximum possible because the restriction of maximum area is active. Therefore, there is no better solution that maximizes the buckling strength without increasing the area over the upper limit.

Table 2 shows results for CC beams under uniformly distributed load of intensity q_y and q_z. Loading with q_y, a box-beam provides

the lowest cost. Therefore, the box section is the best solution if the aim of the design is to maximize the resistance to buckling, with minimum weight. That optimal solution also gives a higher strength. The cost for a C-beam is always much greater than for the other two beams. This is because the resistance to both global and local buckling of the C-beam is lower with respect to a I or a box-beam. For this loading case (q_y), the local buckling and maximum area restrictions are active while the other conditions are verified.

For CC box and I beams loaded with q_z, the design is restricted by the extreme values of the range in which b and h are defined. Also for this loading case, Table 2 shows that resistance to buckling is slightly lower for the I-beam than for the box-beam, but the optimal cross-sectional area is considerably lower. Consequently, the I-beam gives the minimum cost (see Eq. (1)) and it must be the preferred design in this case. Note that for C-beams loaded with q_z the local buckling is an active restriction. This results in an optimal section with a high thickness and the design is no longer constrained by the extreme values of the range in which b and h are defined.

Fig. 11 shows the values of the objective function when the solution is close to (but different from) the optimal solution. Only the design variables varied from the optimal are indicated. It can be seen that small changes in the variables b and h produce a similar value of objective function (in that sense, the optimal solution appears to be robust). On the other hand, modifying the number of layers or the fiber orientation produces a great variation of the objective function. This is logical since changing the laminate or the number of layers represents a much more dramatic modification of the structure than changing b or h.

Total average computation time is around 50 min (Calculations are performed with a Dual Core Intel Wolfdale 2533 MHz processor with 2 Gb of RAM). For some cases, the design is only restricted by the extreme values of b and h and therefore the range of feasible solutions increases. This produces a more expensive optimization problem, with increasing computation times (up to 130 min). The initial parameters of the SA algorithm are set as: $r=100$, $T_{min}\in(1\,10^{-12}, 1\,10^{-16})$. Various calculations are performed until the best converge is achieved. Convergence is reached for each optimization scenario under study. As an example, Fig. 12 shows the best convergence of the algorithm for the design of a SS box-beam under q_z loading (First case of Table 1).

6. Conclusions

In this paper, a new methodology based in the Simulated Annealing method is presented to optimize the design of thin-walled composite beams. The objective function is defined in order to simultaneously maximize the global buckling load and minimize the weight of the beam. The cross-section dimensions and the laminate stacking sequence are optimized for particular design requirements. A complete set of restrictions were considered, including global and local buckling, strength condition and geometric requirements.

As an example, box, C and I sections were studied, searching for the optimal design which provides a high global buckling load while afford low weight, considering different design conditions. The optimal solutions are those which minimize an objective function, and also verify the restrictions for every condition proposed. It is shown that, given a specific design requirement, the selection of the optimal configuration may be a complex problem, involving several variables and possible solutions. Therefore, a design scheme formulated as an optimization problem, such as presented in this paper, represents a significant aid in the design process of this kind of slender structures.

Acknowledgment

The authors would like to thank support of Secretaría de Ciencia y Tecnología de la Universidad Tecnológica Nacional (PID 25/B026) and CONICET (Exp. 3759/13). Florencia Reguera also would like to thank Professor Franco Dotti for his valuable comments and suggestions. The present work is part of the doctoral thesis by Florencia Reguera, under the direction of Víctor Cortínez and Marcelo Piovan, at the Engineering Department of Universidad Nacional del Sur.

Appendix A. Volume and surface initial forces.

The volume initial forces defined in Eq. (14) are expressed as

$$q_2^0 = \int_A \left[-\bar{y}F_y^0\theta_z - \frac{\left(\bar{y}F_z^0 + \bar{z}F_y^0\right)}{2}\theta_y + \frac{zF_x^0}{2}\phi_x \right] dnds,$$

$$q_3^0 = \int_A \left[-\frac{\left(\bar{y}F_z^0 + \bar{z}F_y^0\right)}{2}\theta_z - \bar{z}F_z^0\theta_y - \frac{yF_x^0}{2}\phi_x \right] dnds,$$

$$q_4^0 = \int_A \left[\frac{zF_x^0}{2}\theta_z - \frac{yF_x^0}{2}\theta_y - \left(\bar{y}F_y^0 + \bar{z}F_z^0\right)\phi_x \right] dnds, \tag{A1}$$

where F_x^0, F_y^0 and F_z^0 are the initial forces per unit volume in the x, y and z directions, respectively. Also, the surface initial forces defined in Eq. (15) are expressed as

$$N_2^0 = \int_A \left[-\bar{y}T_y^0\theta_z - \frac{\left(\bar{y}T_z^0 + \bar{z}T_y^0\right)}{2}\theta_y + \frac{zT_x^0}{2}\phi_x \right] dsdn,$$

$$N_3^0 = \int_A \left[-\frac{\left(\bar{y}T_z^0 + \bar{z}T_y^0\right)}{2}\theta_z - \bar{z}T_z^0\theta_y - \frac{yT_x^0}{2}\phi_x \right] dsdn,$$

$$N_4^0 = \int_A \left[\frac{zT_x^0}{2}\theta_z - \frac{zT_x^0}{2}\theta_y - \left(\bar{y}T_y^0 + \bar{z}T_z^0\right)\phi_x \right] dsdn, \tag{A2}$$

where T_x^0, T_y^0 and T_z^0 are the initial applied forces per unit area in the x, y and z directions, respectively.

References

[1] V. Savic, M.E. Tuttle, Z.B. Zabinsky, Optimization of composite I-sections using fiber angles as design variables, Compos. Struct. 53 (2001) 265–277, http://dx.doi.org/10.1016/S0263-8223(01)00010-1.
[2] O. Erdal, F.O. Sonmez, Optimum design of composite laminates for maximum buckling load capacity using simulated annealing, Compos. Struct. 71 (2005) 45–52, http://dx.doi.org/10.1016/j.compstruct.2004.09.008.
[3] G. Narayana Naik, S. Gopalakrishnan, R. Ganguli, Design optimization of composites using genetic algorithms and failure mechanism based failure criterion, Compos. Struct. 83 (2008) 354–367, http://dx.doi.org/10.1016/j.compstruct.2007.05.005.
[4] E. Magnucka-Blandzi, Effective shaping of cold-formed thin-walled channel beams with double-box flanges in pure bending, Thin Wall Struct. 49 (1) (2011) 121–128, http://dx.doi.org/10.1016/j.tws.2010.08.013.
[5] N.R. Bauld, L.S. Tzeng, A Vlasov theory for fiber-reinforced beams with thin-walled open cross sections, Int. J. Solids Struct. 20 (3) (1984) 277–297, http://dx.doi.org/10.1016/0020-7683(84)90039-8.
[6] O. Song, L. Librescu, Free vibration of anisotropic composite thin-walled beams of closed cross-section contour, J. Sound Vib. 167 (1) (1993) 129–147, http://dx.doi.org/10.1006/jsvi.1993.1325.
[7] J.C. Massa, E.J. Barbero, A strength of materials formulation for thin-walled composite beams with torsion, J. Compos. Mater. 32 (17) (1998) 1560–1594, http://dx.doi.org/10.1177/002199839803201702.
[8] J. Loughlan, Multi-cell carbon fibre composite box beams subjected to torsion with variable twist, Thin-Walled Struct. 46 (2008) 914–924, http://dx.doi.org/10.1016/j.tws.2008.01.010.
[9] C.N. Chen, Dynamic equilibrium equations of composite anisotropic beams considering the effects of transverse shear deformations and structural

damping, Compos. Struct. 48 (2000) 287–303, http://dx.doi.org/10.1016/S0263-8223(99)00117-8.
[10] X.X. Wu, C.T. Sun, Vibration analysis of laminated composite thin walled beams using finite elements, AIAA J. 29 (5) (1991) 736–742, http://dx.doi.org/10.2514/3.10648.
[11] V.H. Cortínez, M.T. Piovan, Vibration and buckling of composite thin-walled beams with shear deformability, J. Sound Vib. 258 (4) (2002) 701–723, http://dx.doi.org/10.1006/jsvi.2002.5146.
[12] V.H. Cortínez, M.T. Piovan, Stability of composite thin-walled beams with shear deformability, Comput. Struct. 84 (2006) 978–990, http://dx.doi.org/10.1016/j.compstruc.2006.02.017.
[13] M.T. Piovan, V.H. Cortínez, Mechanics of shear deformable thin-walled beams made of composite materials, Thin Wall Struct. 45 (1) (2007) 37–62, http://dx.doi.org/10.1016/j.tws.2006.12.001.
[14] Z. Kolakowski, A. Teter, Static interactive buckling of functionally graded columns with closed cross-sections subjected to axial compression, Compos. Struct. 123 (2015) 257–262, http://dx.doi.org/10.1016/j.compstruct.2014.12.051.
[15] J. Loughlan, N. Yidris, The local-overall flexural interaction of fixed-ended plain channel columns and the influence on behaviour of local conditions at the constituent plate ends, Thin-Walled Struct. 81 (2014) 132–137, http://dx.doi.org/10.1016/j.tws.2014.02.028.
[16] P. Qiao, L. Shan, Explicit local buckling analysis and design of fiber-reinforced plastic composite structural shapes, Compos. Struct. 70 (2005) 468–483, http://dx.doi.org/10.1016/j.compstruct.2004.09.005.
[17] G. Tarján, Á. Sapkás, L.P. Kollár, Local web buckling of composite (FRP) beams, J. Reinf. Plast. Comp. 29 (2009) 1451–1462, http://dx.doi.org/10.1177/0731684409105083.
[18] K. Magnucki, M. Maćkiewicz, J. Lewiński, Optimal design of a mono-symmetrical open cross section of a cold-formed beam with cosinusoidally corrugated flanges, Thin Wall Struct. 44 (2006) 554–562, http://dx.doi.org/10.1016/j.tws.2006.04.016.
[19] S.W. Tsai, E.M. Wu, A general theory of strength for anisotropic materials, J. Compos. Mater. 5 (1971) 58–80, http://dx.doi.org/10.1177/002199837100500106.
[20] V.Z. Vlasov, Thin-walled Elastic Beams, Program for Scientific Translations, Jerusalem, Israel, 1961.
[21] K. Washizu, Variational Methods in Elasticity and Plasticity, Pergamon Pr, UK, 1975.
[22] L.P. Kollár, G.S. Springer, Mechanics of Composite Structures, Cambridge University Pr, New York, 2003.
[23] S. Kirkpatrick, C.D. Gelatt, M.P. Vecchi, Optimization by simulated annealing, Science 220 (4598) (1983) 671–680, http://dx.doi.org/10.1126/science.220.4598.671.
[24] A.B. Verdiell, M.C. Maciel, M.C. Vidal, An improved scheme for accelerating the convergence of the simulated annealing algorithm applied to real world problems, Proc. Appl. Math. Mech. 7 (1) (2007) 1060405–1060406, http://dx.doi.org/10.1002/pamm.200700541.
[25] J. Dréo, A. Pétrowski, P. Siarry, E. Taillard, Metaheuristics for hard optimization, Springer-Verlag Berlin Heidelberg, Germany, 2006.